Open Ceramics 5 (2021) 100072

Contents lists available at ScienceDirect

Open Ceramics

journal homepage: www.editorialmanager.com/oceram

Sintering of mixed Ca–K–Na phosphates: Spark plasma sintering vs flash-sintering

N. Orlov [a,c,*], A. Kiseleva [a], P. Milkin [a], P. Evdokimov [a,b], V. Putlayev [a,b], J. Günster [c], M. Biesuz [d], V.M. Sglavo [d], A. Tyablikov [b]

[a] Department of Materials Science, Lomonosov Moscow State University, Moscow, 119991, Russia
[b] Department of Chemistry, Lomonosov Moscow State University, Moscow, 119991, Russia
[c] Federal Institute for Materials Research and Testing (BAM), Unter den Eichen 44-46, Berlin, 12203, Germany
[d] University of Trento, Department of Industrial Engineering, Via Sommarive 9, 38123, Trento, Italy

ARTICLE INFO

Keywords:
Calcium phosphates
Ceramic
Flash-sintering
Spark plasma sintering

ABSTRACT

A comparison between different field-assisted sintering methods (FAST), namely Spark Plasma Sintering (SPS) and flash-sintering (FS), is reported for calcium and alkaline phosphates especially with regards to their microstructure. A reduced average grain size upon SPS is shown when pressure is decreased. Shrinkage curves during flash sintering are compared with similar conventional sintering curve. Flash sintered ceramics possess unusual microstructural features, including a density/grain size gradient where the surface of the specimen is denser and possesses a coarser grains with respect to the core. Such microstructural gradient is opposite to what generally observed, the surface being colder due to the heat radiation toward the environment. The change in the average grain size for each sintering method is related to the process parameters.

1. Introduction

Sintering of calcium phosphates for bone implants is still a non-trivial task despite a fairly large number of publications on this topic [1–4]. This problem is especially acute in the case of substituted calcium phosphates, which show a suitable level of resorption in the body and also have sufficient strength to produce bone replacement implants.

However, obtaining strong ceramics based on substituted Ca–K–Na phosphate is challenging because of the difficulties of their sintering. The main difficulty in sintering is the predominance of recrystallization processes over densification. Grains grow fast because at high temperature (above 600 °C) these materials become cationic-conductors [5]. At the same time, phosphate-anions do not have to move, they just have to reorient to start to belong another grain. However, densification process goes very slow because here phosphates diffusion plays more important role while their mobility is still much lower comparing to cation mobility. The noticeable difference in mobility between cations such as calcium, potassium and sodium and phosphate anions was shown and discussed in numerous works concerning alkali metals and phosphate based ceramic conductors [5–8]. As a result, the microstructure of the resulting ceramics consists of relatively large grains, and pores are observed in a significant amount [5,9,10]. To improve densification, pores should go out of grains to dissolve on a grain boundary but, due to fast coarsening and relatively low mobility of big phosphate anions, pore-grain boundary separation occurs, and they do not stay on grain boundary enough time to dissolve.

Possible methods for solving this problem have been discussed for a long time in the scientific literature. As such, it was proposed to use both modifications of traditional consolidation methods (for example, multi-step sintering [11,12], reaction sintering [10,13]) and methods involving additional factors, for example, an electromagnetic field - FAST (Field Assisted Sintering Techniques) methods - such as Spark Plasma Sintering (SPS) [14–18] and Flash Sintering (FS) [19–23]. SPS is a consolidation technology where a moderate electric potential (<10V) is used to Joule heat a graphite die that contains the ceramic powder, while an external pressure is applied to promote densification. Being the electric potential quite low, most of the electric current passes through the graphite die when processing ceramic materials. Conversely, FS is a pressureless technique which adopts much larger electric field (from a few to 10^3 V/cm). In FS experiments whole the electric current is forced to pass through the ceramic while sintering.

The multi-step sintering allows to form grains contact and stop exceed

* Corresponding author. Leninskiye gory 1-3, r. 449, 119991, Moscow, Russia.
E-mail address: nicolasorlov174@gmail.com (N. Orlov).

https://doi.org/10.1016/j.oceram.2021.100072
Received 15 November 2020; Received in revised form 2 February 2021; Accepted 3 February 2021
Available online 8 February 2021

Table 1
Characteristics of phase transitions in $CaK_{0.6}Na_{0.4}PO_4$ taken from Ref. [5].

	$T_{p.t.}$, °C	$\Delta V_{p.t.}$, %	$\Delta H_{p.t.}$, kJ/mol
$CaK_{0.6}Na_{0.4}PO_4$	667	−0,1	1,4

coarsening and simultaneously maintain the densification by decreasing sintering temperature. However, in case of mixed calcium and alkali metals phosphates which are ion conductor above 660°C coarsening always prevails over densification [5]. As a result, it is not possible to reach the temperature at which the predominant mechanism changes and the pores begin to dissolve faster than grain growth occurs [24].

In contrast to conventional sintering, consolidation methods using an electric field are distinguished by the fact that, in addition to the temperature factor, sintering is promoted by the application of electric current and field. In the case of SPS, densification is further enhanced by the external pressure which increases the driving force for sintering. The result is, in many cases, a significant densification of the ceramic without noticeable grain growth. Thus, model ceramic systems such as Al_2O_3 [25,26], ZrO_2 [27–29], and also compounds with apatite structure such as HA were effectively densified (relative density > 95%) in the minutes timescale maintaining nanometric grains [15,16,23,30,31]. Recent studies [30,32–35] have shown that similar methods can also be successfully applied to tricalcium phosphate, which raises the question of the possible expediency of their application for the preparation of dense ceramics based on mixed calcium and alkali metal phosphates.

The aim of the present work is to compare two different field-assisted sintering technologies, namely spark plasma sintering and flash sintering, for the consolidation of phosphate ceramics with $CaK_{0.6}Na_{0.4}PO_4$ composition. Such material is a promising formulation to make resorbable bioceramics for bone tissue regeneration.

2. Experimental procedures

To determine the possibility of using spark plasma sintering and flash sintering to obtain dense ceramics based on mixed calcium and alkali metal phosphates, the model composition $CaK_{0.6}Na_{0.4}PO_4$ was chosen due to the fact that it has only one phase transition at 667 °C with minimal negative volumetric effect (Table 1) (which was established quite accurately in Refs. [5,36,37] by dilatometry and measuring the temperature dependence of conductivity (Fig. 1a). Moreover, there is room for solid solution based on β-$CaK_{0.6}Na_{0.4}PO_4$ spread in the widest part between $CaK_{0.38}Na_{0.62}PO_4$ and $CaK_{0.82}Na_{0.18}PO_4$ (Fig. 1b).

In addition, this compound contains all types of ions that are usually present in substituted calcium-phosphate ceramics - calcium, potassium, sodium and phosphate (Fig. 1c), which makes it possible to study the effect of each of them on the sintering process, namely, their diffusion mobility upon sintering and promoting densification.

Mixed ternary phosphate β-$CaK_{0.6}Na_{0.4}PO_4$ was synthesized from Sigma-Aldrich precursors (p.a.) via the following reactions:

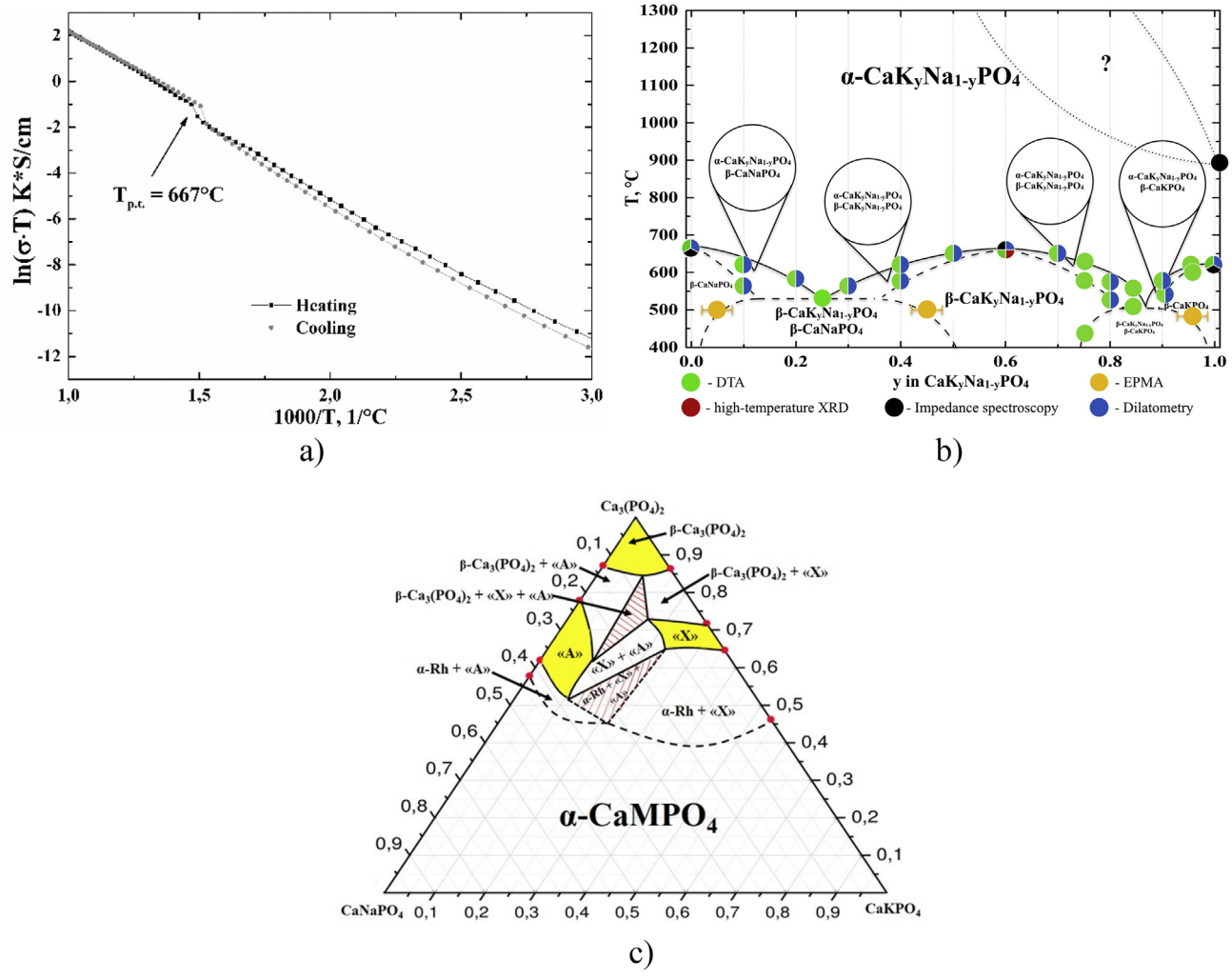

Fig. 1. a) Arrhenius plots for ionic conductivity in $CaK_{0.6}Na_{0.4}PO_4$ (taken from Ref. [5] with small changes), phase diagrams b) $CaNaPO_4$ - $CaKPO_4$ (taken from Ref. [5] with small changes), c) $Ca_3(PO_4)_2$ – $CaNaPO_4$ - $CaKPO_4$ (T = 1200°C) (taken from Ref. [9] with small changes).

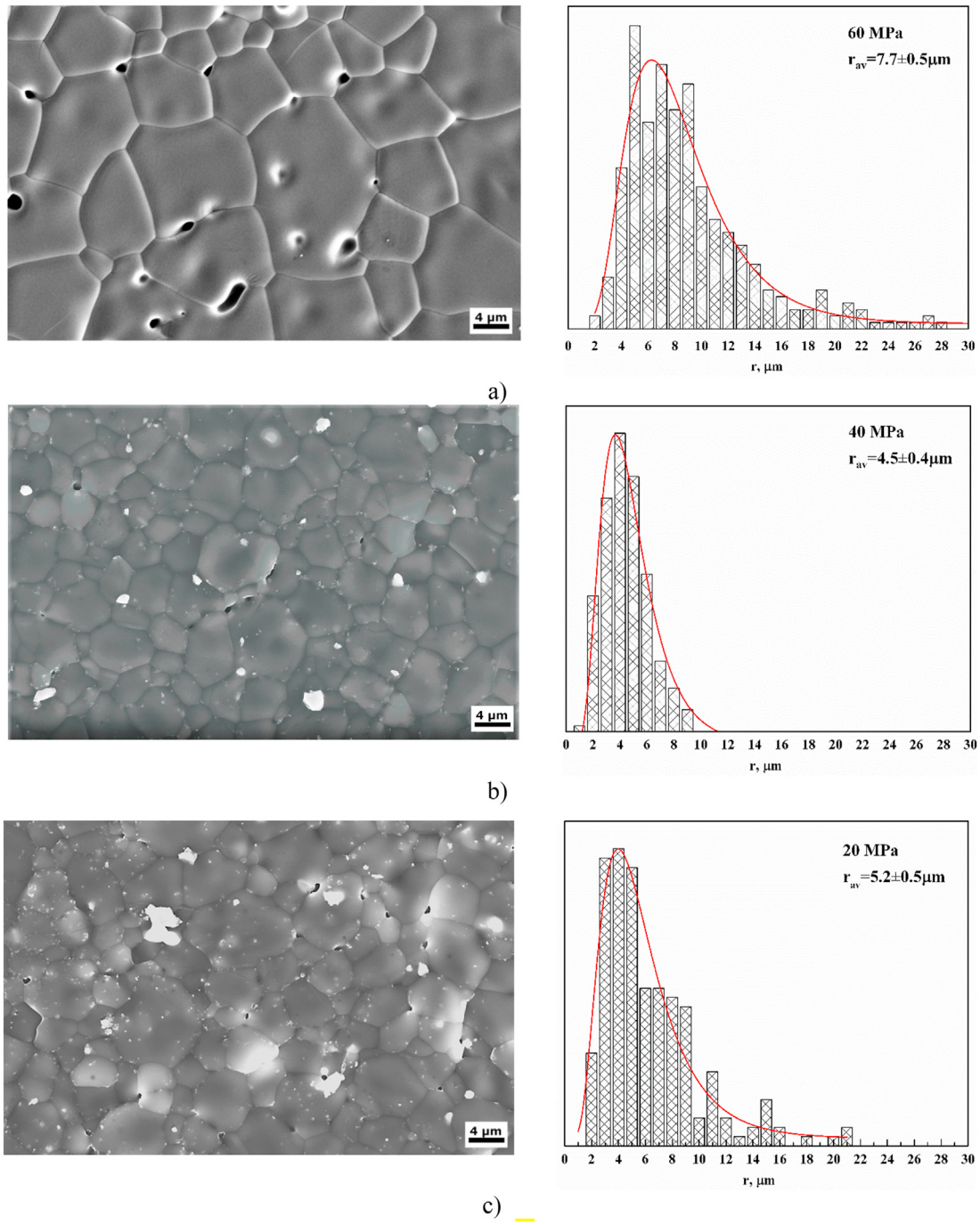

Fig. 2. Microstructure and grain size distribution of β-$CaK_{0.6}Na_{0.4}PO_4$ ceramics after SPS at different pressures a) 60MPa, b) 40MPa, c) 20MPa.

Table 2
β-$CaK_{0.6}Na_{0.4}PO_4$ ceramic characteristics after conventional and two-step sintering [5].

	Schedule	Relative density, %	Average grain size, μm
Conventional sintering	1200°C, 12 h	92%	20
Two-step sintering	1200°C, 0 min, 1100°C, 48 h	85%	20

1) $Ca(NO_3)_2 + (NH_4)_2HPO_4 \rightarrow CaHPO_4{\cdot}H_2O + 2NH_4NO_3$ (in water solution)
2) $2CaHPO_4{\cdot}H_2O \rightarrow Ca_2P_2O_7 + 2H_2O\uparrow$ (T = 700 °C)
3) $Ca_2P_2O_7 + CaCO_3 \rightarrow Ca_3(PO_4)_2 + CO_2\uparrow$ (T = 900 °C)
4) $Ca_2P_2O_7 + Na_2CO_3 \rightarrow 2CaNaPO_4 + CO_2\uparrow$ (T = 900 °C)
5) $Ca_2P_2O_7 + K_2CO_3 \rightarrow 2CaKPO_4 + CO_2\uparrow$ (T = 900 °C)
6) $0.6CaKPO_4 + 0.4CaNaPO_4 \rightarrow$ β-$CaK_{0.6}Na_{0.4}PO_4$ (T = 900 °C)

The synthesis of mixed ternary phosphate has been described in detail in previous works [5]. First brushite was synthesized in water solution from the soluble salts calcium nitrate ($Ca(NO_3)_2{\cdot}4H_2O$, 0.6 M) and ammonium hydrophosphate ($(NH_4)_2HPO_4$, 0.6 M) and then calcium pyrophosphate was obtained by firing at 700 °C. Tricalcium phosphate and potassium and sodium rhenanites were obtained by mixing calcium pyrophosphate with the respective carbonates and then firing at 900 °C,

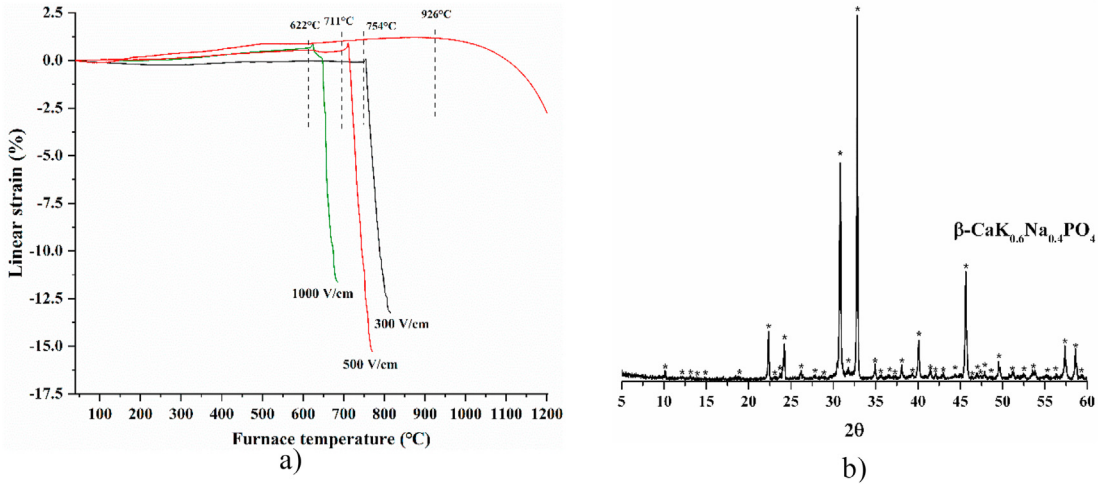

Fig. 3. a) Linear strain during flash sintering and conventional sintering vs furnace temperature; b) XRD of the sample after flash-sintering at 1000 V/cm (* - peaks specific to the low-temperature phase).

from which mixed calcium and alkali phosphates were obtained by firing at 900 °C.

The mixtures of reactions 2–6 were ground in a planetary ball mill (Pulverisette, Fritsch, Germany) for 10 min (4000 rpm) in an acetone medium and then dried in air and calcined in Al_2O_3 crucibles. The obtained powders were analyzed by XRD analysis.

In the SPS approach, β-$CaK_{0.6}Na_{0.4}PO_4$ powder was consolidated in a LABOX-625 SinterLand Inc. (Japan) system into a graphite mold with an inner diameter of 10 mm. To protect the surface of the mold, graphite paper was placed between the inner walls of the mold and the powder. Sintering was carried out at various pressures (20, 40, and 60 MPa) and a temperature of 970 °C (heating rate from 600 °C was 120 K/min and dwelling time 4 min). The temperature was measured with a pyrometer on the surface of the mold at 360 mm from the die.

Flash sintering was carried out in a modified Linseis L75 dilatometer (Germany) with a constant heating rate of 20 K/min. The powders were pressed using a Carver press (USA) into cylinders with 5 mm diameter and 7 mm height. A 5% solution of polyethylene glycol in water was used as a plasticizer. The uniaxially pressed pellets were placed in the dilatometer between two Pt–Rh disks acting as electrodes. To improve the ceramic/metal electric contact, Ag paste was spread on the parallel, flat faces of the pellets. A DC field was applied using a Glassman EW series 5 kV–120 mA (Singapore) power supply. The electric potential was applied when the sample reached 350 °C and it was maintained until the current limit was reached. The imposed field ranged from 300 to 1000 V/cm until the set current limit value (120 mA, corresponding to 6 mA/mm^2) was achieved. After reaching the set current, the power source switched to the current control mode and the current was allowed to flow for 2.5 min. The current and voltage were recorded using a KEITHLEY 2100 6½ Digit Multimeter (USA).

The crystalline phase compositions and unit cell parameters were studied via X-ray diffraction (XRD), which was performed using a diffractometer with a rotating anode (D/Max- 2500, Rigaku, Japan). Spectra were acquired in reflection mode (Bragg-Brentano geometry for reflection) using Cu Kα radiation (wavelength = 1.54183 Å).

Bulk and apparent densities, as well as the open porosity, were determined by the Archimedes' technique according to ISO 18754:2013:Method B. For the experiment, scales (Sartorius, Germany) with a hydrostatic weighing frame were used. Filling the pores of the samples was carried out under vacuum.

To study the microstructures of the sintered bodies, the samples were polished (DAP-V/Pedemin, Struers, Denmark, and TegraPol-11, Struers, Denmark) with an automatic rotating sample holder (TegraForce-1, Struers, Denmark) according to method F of the user manual (Metalog Guide, Struers, Denmark). Polished surface was thermally etched at 900°C for 30 min.

The samples were observed on a LEO SUPRA 50VP scanning electron microscope (SEM) with a field emission gun (Carl Zeiss, Germany), as well as by a NVision 40 SEM (Carl Zeiss, Germany) using a SE2 secondary electron detector. A layer of carbon or chromium was preliminarily deposited on the samples (Quorum Technologies deposition device, QT-150T ES, United Kingdom). X-ray microanalysis with energy dispersion (EDX) was performed on a SUPRA 50VP microscope equipped with the INCA Energy 300 microanalysis system (Oxford Instruments, United Kingdom) at accelerating voltage of 20 kV. Ca Kα, P Kα, Na Kα, and K Kα spectral lines were chosen for the analysis. Matrix correction was carried out using ϕ(ρz) – technique in XPP-modification.

The measurement of grain sizes was carried from SEM images by measuring the area of the grain in ImageJ software and then calculating the radius of the circle of the corresponding area. To construct histograms, at least 100 particles were measured.

3. Results and discussion

The microstructures of β-$CaK_{0.6}Na_{0.4}PO_4$ ceramic samples after SPS are shown in Fig. 2.

It can be observed that the density of the mixed phosphates obtained by SPS (c.a. 97% of the theoretical one) significantly exceeds that of those obtained by conventional sintering that typically ranges from 85 to 92% (Table 2) [5]. In addition, the microstructure of the SPSed ceramics shows a small number of pores, which are located mainly at the grain boundaries and triple junctions. This situation is undoubtedly favorable for further densification of the ceramics [24].

In agreement with previous research activities it is shown that the grain size increases with pressure especially at 60 MPa. The relative density of all samples is 97 ± 1%. The microstructure (Fig. 1) gives again an evidence of the presence of pores at grain boundaries.

Faster grain growth with increasing pressure and wide grain size distribution at 60 MPa (which is opposite to common experience from hot pressing [38]) is described in several works [39–42]. The origin is not clear but one of possible explanation of this phenomenon could be a plastic deformation of grains as well by their sliding and rotation. Along with atom jumps across the grain boundary this leads to diminishing in misorientation of contiguous grains and, therefore, to faster boundary movement. In fact, coalescence of neighboring grains takes place. In a single-phase material, the existence of different grains is explained by the different orientations of the crystallographic planes. In the process of applying pressure, the grains shift relative to each other with

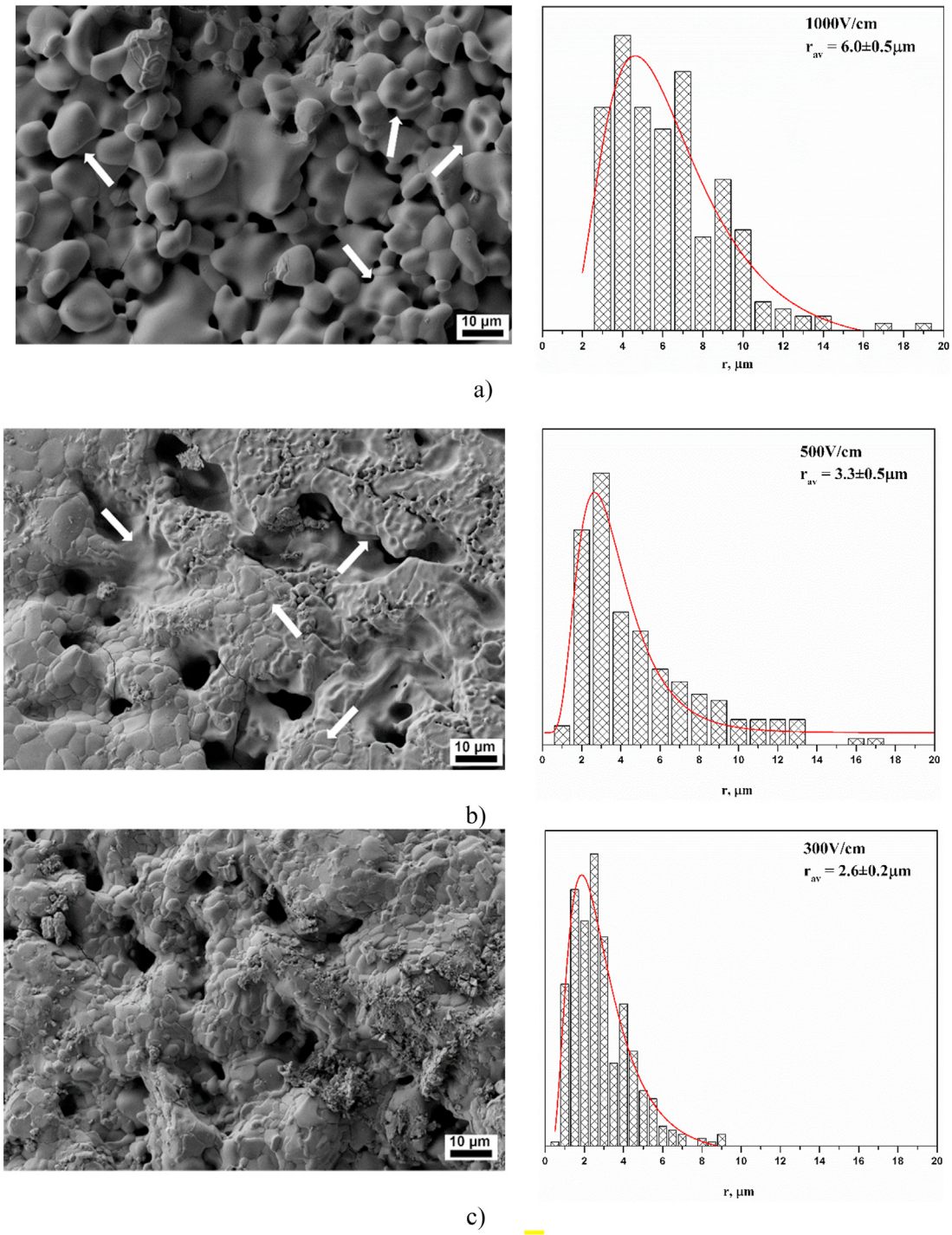

Fig. 4. Microstructure and grain size distribution of β-$CaK_{0.6}Na_{0.4}PO_4$ ceramics after flash-sintering at different field strength a) 1000V/cm, b) 500V/cm, c) 300V/cm. Arrows show a few examples of melted places without sharp edges and with uniform continuous material between grains.

simultaneous plastic deformation. As a result of this movement of grains or the displacement of some of the atoms into the grain boundary region, the planes of two neighboring grains can become oriented in the same way, which, with subsequent small diffusion of atoms, leads to the formation of large grains. With increasing pressure, these grains unification are more intensive, especially in ionic bodies with rather weak energy of crystal lattice where ion diffusion is even more active (this is the case for $CaK_{0.6}Na_{0.4}PO_4$, see e.g. Ref. [43]), which is the reason for the results in Fig. 2.

Another explanation of the effect expects that with increasing pressure the onset of sintering is anticipated. Indeed, grain coarsening could not take place via solid state diffusion until necks are formed (unless other phenomena like evaporation/condensation are activated). Since the sintering cycle was the same for all pressure values, the sample treated at 60 MPa has, in fact, "more time" to coarse its microstructure. However, in the case of the SPS experiments described above holding at a given temperature (as well as heating time) consists several minutes (4 min for holding and 3 min for heating from 600 to 970 °C). Therefore, the difference in time for grain growth at different pressures occupies also few minutes.

The results indicate that a significant improvement in densification of mixed Ca–K–Na phosphates is achieved by SPS which appears not only

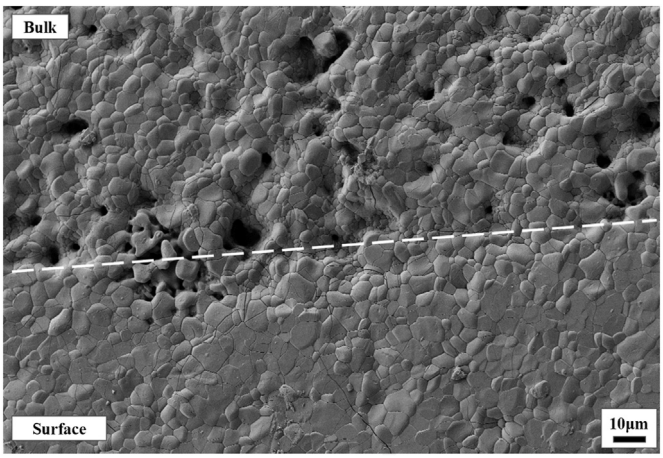

Fig. 5. Microstructure of near-the-surface region of β-$CaK_{0.6}Na_{0.4}PO_4$ ceramics after flash-sintering (300V/cm).

related to the external pressure application but could involve additional factors like high heating rate and possible athermal field-activated phenomena. It was mentioned above (Fig. 1a) that the $CaK_{0.6}Na_{0.4}PO_4$ demonstrates weak ionic conductivity even after phase transition [5]. As a result, under SPS conditions, very limited current flows through the sample, it passes mainly through graphite mold. In this sense, the reason for better sintering of the mixed phosphates under SPS could be the fast heating caused by the contact with the hot walls of the mold. It is also worth considering the possibility of the effect of electrical field on the diffusion processes during sintering even in the absence of a significant current through the sample.

It should be noted that there is a significant difference in the field strength and applied current in the case of SPS and flash sintering. In the case of SPS, small values of the field are used, but the current can reach a few thousand amperes (in the graphite die). While in flash sintering, at least small currents (hundreds of mA) and hundreds of volts of field strength are applied directly to the ceramic. The nature of field assistance to sintering is still debatable and several mechanisms have been proposed, including (i) thermal runaway caused by Joule heating [44], (ii) localized grain boundary overheating/melting [45]; (iii) field-assisted Frenkel's pairs nucleation [19,27,44]; (iv) electrochemical phenomena [46,47], and (v) thermodiffusion [48]. In order to study effect of the current flowing through the sample during sintering, the samples were also subjected to flash sintering. The shrinkage curves are shown in Fig. 3a.

Upon heating, the flowing current increases leading to fast heating of the sample and, therefore, to thermal expansion. This is clearly visible on the dilatometric curves as small expansions just at flash event followed by a stage of sharp shrinkage. One can observe that the highest the applied voltage, the lowest the sintering onset temperature, which ultimately leads to the onset temperature below the β→α phase transition temperature ($T_{ph.t.} = 670$ °C). The slope modification of the sintering curve at 1000 V/cm probably corresponds to the moment of the phase transition. The XRD analysis of the samples after sintering show the presence of low-temperature β-$CaK_{0.6}Na_{0.4}PO_4$ only (Fig. 3b).

The microstructure the FSed samples is shown in Fig. 4. One can observe that sintering under high fields (1000V/cm and 500V/cm) traces of melt are visible. Thus, grains have no sharp edges, the surface is very smooth and there is uniform continuous phase between grains after 500V/cm (a few examples are represented by arrows in microstructures, Fig. 4 a, b). However, the number of pores is lower compared to the microstructure after conventional sintering. At the same time, the large size of the round particles (6.0 ± 0.5 μm) and, at the same time, the small area of interconnections between them at 1000 V/cm correspond to liquid-phase sintering. Observed melting stems between grains could be initiated by intensive thermal runaway during flash event in the field of 1000 V/cm. In a previous work [5], we concluded that in Ca–K–Na phosphate ceramics recrystallization processes prevail over densification. However, the use of fast-firing techniques (i.e., high heating rate) allows enhanced consolidation. During FS, high heating rates are achieved, and this can be considered beneficial for sintering. But, the thermal runaway at 1000 V/cm was probably too intense leading to the formation of a

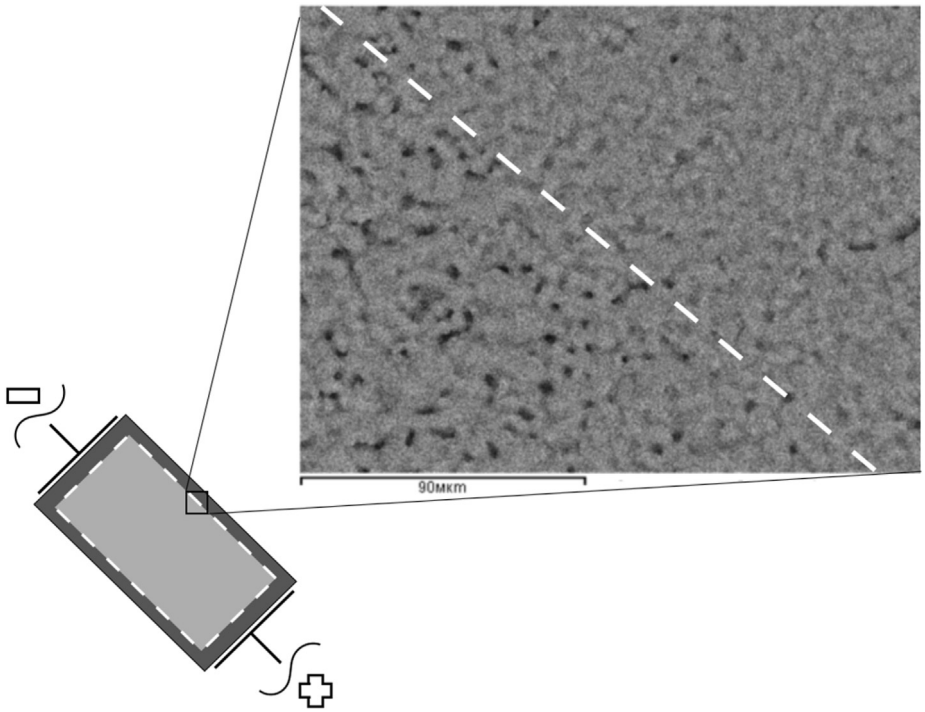

Fig. 6. Non-uniform sintering of the ceramic at 300 V/cm; the rectangular area taken from the border between dense near-the-surface area and less dense core demonstrates different microstructure.

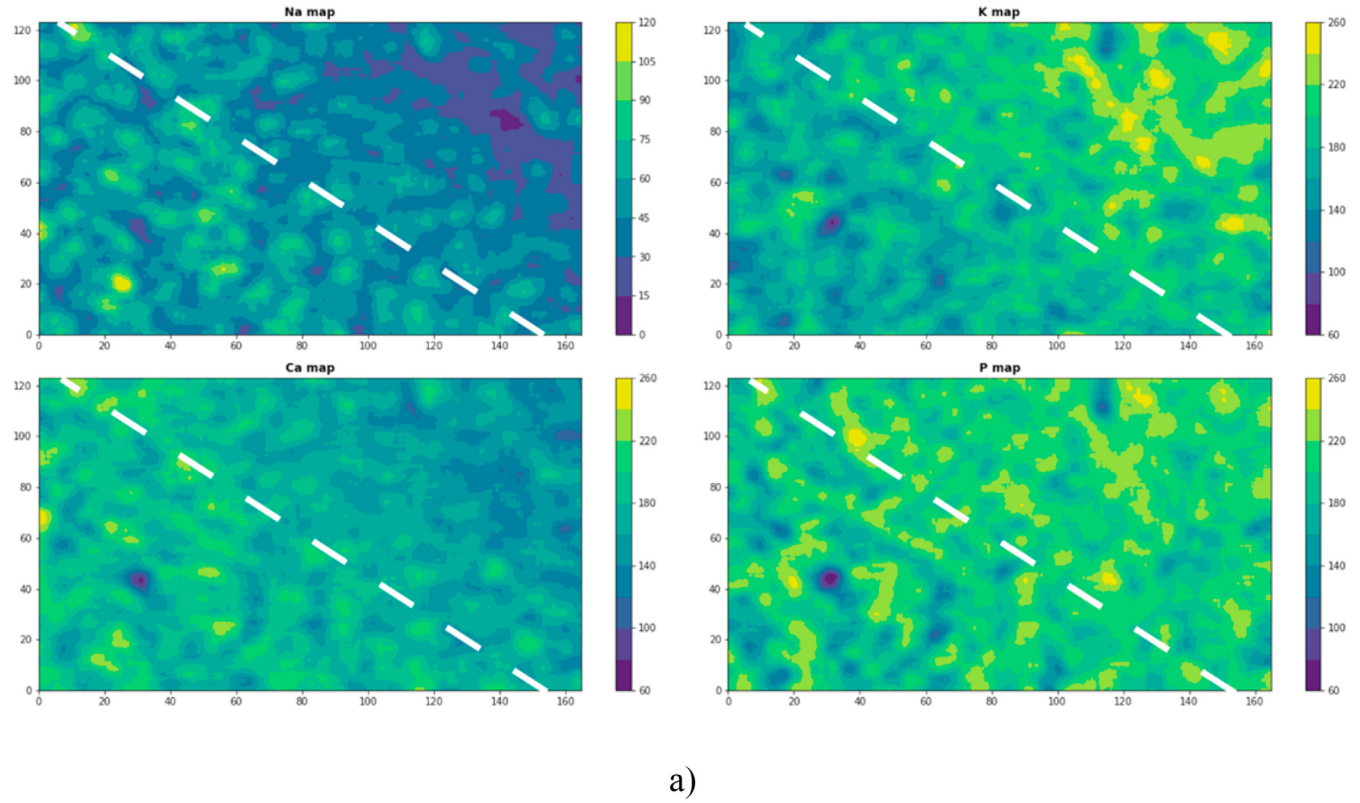

a)

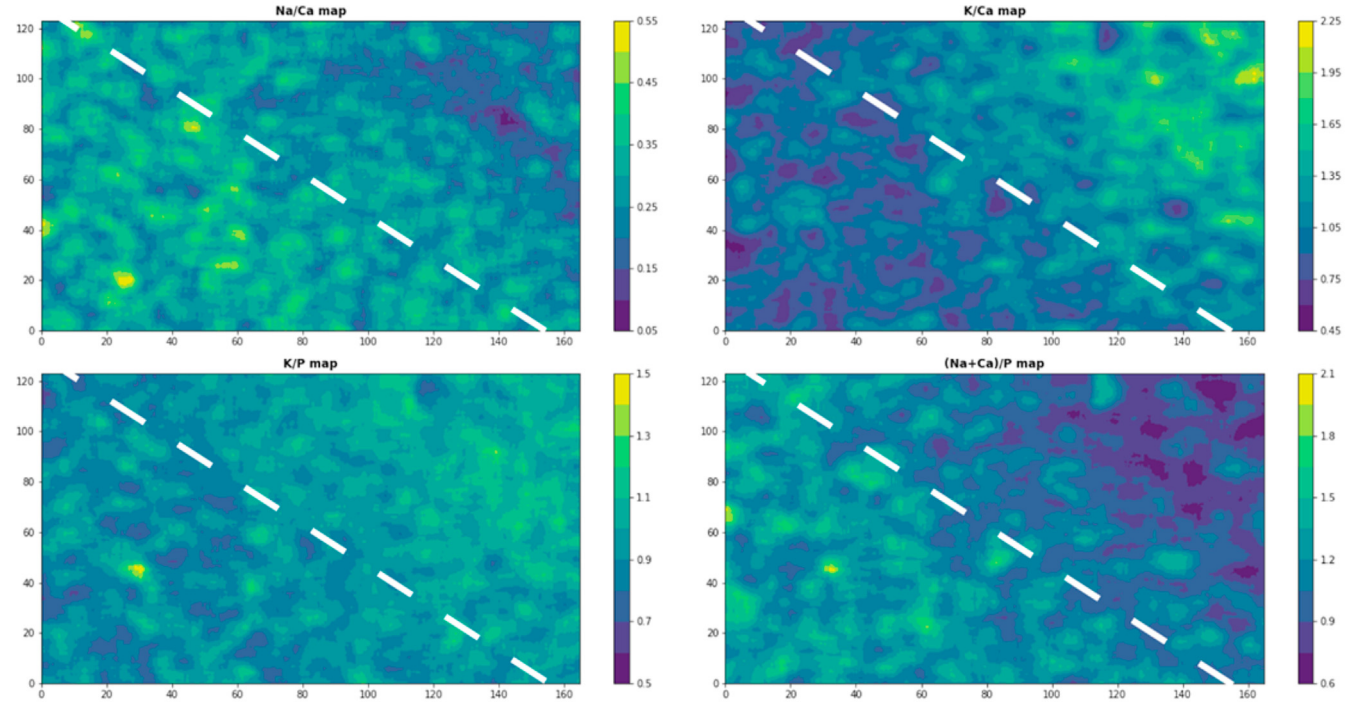

b)

Fig. 7. EDXS elements distribution maps at the border between core and dense regions (from the rectangular area depicted in Fig. 6); the relative amount of elements or their combinations can be recognized using color scale-bars (arbitrary units). (For interpretation of the references to color in this figure legend, the reader is referred to the Web version of this article.)

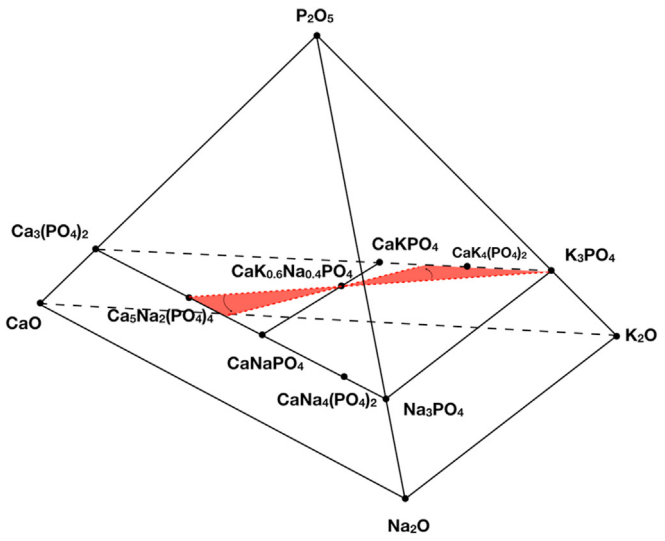

Fig. 8. Phase relationships (schematically) in the system P_2O_5–CaO–Na_2O–K_2O (the red area includes possible pathes of $CaK_{0.6}Na_{0.4}PO_4$ decomposition during flash-sintering). (For interpretation of the references to color in this figure legend, the reader is referred to the Web version of this article.)

liquid phase. From this viewpoint, moderate fields (300V/cm or even less) better suit for solid-state sintering of $CaK_{0.6}Na_{0.4}PO_4$ ceramic.

It is also interesting to observe that flash sintering of this particular ceramic proceeds non-uniformly. In the near-the-surface region in curve sample side, the sample is denser than in the remaining volume (Fig. 5), this probably indicating a temperature difference in the specimen. The thickness of such shell is nonuniform through the sample and does not depend on field strength. In average it is in range of 50–150μm. Generally speaking, the microstructure of the core can be attributed to incomplete sintering. It looks like if sintering proceeds from the surface to the core of the sample. Well discernible sintering front sweeps out pores like a grain boundary during boundary control regime of sintering. This is evidenced by the attachment of pores to the interface of sintering front and partial coalescence of pores in the core area (Figs. 5 and 6). Neglecting preferred path of current through the surface region (leading to overheating the surface), one should conclude that due to thermal runaway in the volume and irradiation from the surface, the core of the sample is hot, and the surface is chiller. Thus, our results showing a higher level of densification/coarsening on the surface (Figs. 5 and 6) which are quite surprising and interesting, revealing a behavior never reported in flash sintered specimen.

One can also attempt to compare the occurrence of the surface dense layer with hot spots formed during flash sintering - places where stochastic variations of the electric current result in stable current concentrations in small overheated spots (i.e., the current fluctuation is stabilized thanks to the negative temperature coefficient for electrical resistivity) [18]. However, the presence of a well-distributed dense region all around the specimen does not match the typical morphological features of the hot spots which involve the overheating of small localized regions (usually in the sample center). We can conclude that the formation of the surface/core microstructural gradient reported in Figs. 5 and 6 is not related to hot spots formation.

To unravel the origin of the surface/core microstructural gradients, EDXS analysis of the sample area including the border between dense and less dense inner parts of the sample (Fig. 6) was carried out.

As one can see from the EDXS maps (Fig. 7), there is a migration of potassium towards a denser region, while sodium and calcium were shifted to a more porous part. At the same time, the intensity of phosphorus signal remained approximately at the same level over the entire area of the analyzed area.

From the point analysis it is possible to estimate roughly the composition variation in the vicinity of the border after flash sintering. In the lower left part of the map, corresponding to a less dense area (the core), the ratio of sodium to calcium is of about 0.4–0.45; the ratio between cations and phosphorus in this region is slightly higher than 1.5. This suggests that the composition is shifted toward the compound $Ca_5Na_2(PO_4)_4$. At the same time, in the upper right part (surface), as already mentioned, there is a larger content of potassium. The ratio of potassium to phosphorus in this area also increases up to 1.3–1.4; the ratio of potassium to calcium is close to 2. According to these ratios, the resulting compositions of these regions lie on the $Ca_5Na_2(PO_4)_4$–K_3PO_4 line, or bearing in mind different diffusivity of Ca, Na, K cations on the curve situated in the vicinity of this line, as it is shown in Fig. 8.

At the sintering temperature (which is higher than the observed flash onset temperature, 754 °C at 300 V/cm, Fig. 3a) $CaK_{0.6}Na_{0.4}PO_4$ composition belongs to extended area of a solid solution of α-Ca(K,Na)PO_4 with glaserite structure (Fig. 1c); the solid solution of this type shows cationic conductivity [5]. If a surface/core themal gradient is established at the flash transition (this is likely because the surface radiate heat toward the environment), there is a possibility of changing the initial uniform composition of the solid solution (demixing) due to thermodiffusion of mobile cationic species (Ludwig-Soret effect). It is known from the theory of thermal diffusion that concentration gradient of each mobile specie caused by temperature gradient can be expressed as (stationary conditions, diluted solution) [49,50]:

$$\frac{dlogC}{dT} = \frac{-Q}{RT^2} \quad (1)$$

where C – local concentration of the diffusant, T – local temperature, R (=8.31 J mol^{-1} K^{-1}) – gas constant, Q – heat of transfer of the specie along gradient. It is accepted that $Q = H_1 - H_2$, where H_1 – enthalpy related to leaving by atom (ion) its regular position, while H_2 – enthalpy related to landing by atom (ion) to a new position along gradient. For light, highly mobile species, usually $H_1 < H_2$, so according to (1) highly diffusive atoms are concentrated in a hot zone (abnormal Ludwig-Soret effect). In the case of $CaK_{0.6}Na_{0.4}PO_4$, in accordance with charge and radius, the ions can be ordered in the following row of decreasing their diffusivity: $Na^+ > Ca^{2+} > K^+$. Taking the above consumptions into account, it is possible to conclude that Na and Ca can concentrate in a hot core, while K goes to chiller surface layer. Better sintering ability of K-rich layer does not contradict our data on sintering of different compositions in $CaNaPO_4$ – $CaKPO_4$ system where K-rich composition demonstrated better densification [5]. Clearly, it is necessary to measure temperature gradient as well as Q values for the diffusants to confirm unambiguously such a conclusion. It is also of interest whether the described demixing of the solid solution in temperature gradient can proceed further leading to a phase separation, i.e. formation of multi-phase mixtures (depicted in Fig. 1c) as it was observed for other materials in gradient of chemical potentials [49,51]. These issues are addressed to a forthcoming paper.

4. Conclusions

The possibility to sinter ceramics based on substituted calcium phosphates $CaK_{0.6}Na_{0.4}PO_4$ to a 96% of relative density and grain size is about 4.5 μm by SPS technique was shown. Grain size of ceramic increases with applied pressure. This phenomenon was explained by plastic deformation of grains as well by their sliding and rotation during sintering under pressure. Materials with an average grain size of about 2.6 μm were obtained by Flash sintering. It was shown higher field strength correspond to lower average grain size. Density difference between the surface of the sample and its core was observed and this was accounted for by radial temperature gradient.

The migration of potassium towards denser region, and sodium/calcium to more porous parts during flash-sintering was revealed. According to observed elemental ratios in the near-the-surface region, the resulting

compositions of these regions lie in the vicinity of $Ca_5Na_2(PO_4)_4$–K_3PO_4 line. The possible explanation can include a thermal diffusion phenomenon (Ludwig-Soret effect).

Acknowledgments

The reported study was funded by RFBR, projects numbers 19-38-90199 and 19-03-00940 and in part by the Lomonosov Moscow State University program of development.

V.M. Sglavo and M. Biesuz kindly acknowledge the support from the Italian Ministry of University and Research (MIUR) within the programs PRIN2017 - 2017FCFYHK "DIRECTBIOPOWER", PRIN2017 - 2017PMR932 "Nanostructured Porous Ceramics for Environmental and Energy Applications" and Departments of Excellence 2018–2022 (DII-UNITN).

Prof. J. Günster and N. Orlov acknowledge State of Lower Saxony, Germany within the PhD Program "Self-organizing multifunctional structures for adaptive lightweight constructions".

References

[1] E. Champion, Sintering of calcium phosphate bioceramics, Acta Biomater. 9 (2013) 5855–5875, https://doi.org/10.1016/j.actbio.2012.11.029.
[2] K. DeGroot, Application of calcium phosphate bioceramics, J. Ceram. Soc. Japan. 99 (1991) 943–953.
[3] L.L. Hench, Bioceramics, J. Am. Ceram. Soc. 81 (1998) 1705–1728.
[4] S. Raynaud, E. Champion, D. Bernache-Assollant, Calcium phosphate apatites with variable Ca/P atomic ratio II. Calcination and sintering, Biomaterials 23 (2002) 1073–1080, https://doi.org/10.1016/S0142-9612(01)00219-8.
[5] N.K. Orlov, P.V. Evdokimov, P.A. Milkin, A.V. Garshev, V.I. Putlayev, V.V. Grebenev, J. Günster, Phase equilibria in $CaNaPO_4$-$CaKPO_4$ system and their influence on formation of bioceramics based on mixed Ca-K-Na phosphates, J. Eur. Ceram. Soc. 39 (2019) 5410–5422, https://doi.org/10.1016/j.jeurceramsoc.2019.07.044.
[6] M. Nagai, Y. Shibuya, T. Nishino, T. Saeki, H. Owada, K. Yamashita, T. Umegaki, Electrical conductivity of calcium phosphate ceramics with various Ca/P ratios, J. Mater. Sci. 26 (1991) 2949–2953, https://doi.org/10.1007/BF01124826.
[7] S. Song, H.M. Duong, A.M. Korsunsky, N. Hu, L. Lu, A Na^+ superionic conductor for room-temperature sodium batteries, Sci. Rep. 6 (2016) 32330, https://doi.org/10.1038/srep32330.
[8] D. Kundu, E. Talaie, V. Duffort, L.F. Nazar, The emerging chemistry of sodium ion batteries for electrochemical energy storage, Angew. Chem. Int. Ed. 54 (2015) 3431–3448, https://doi.org/10.1002/anie.201410376.
[9] N.K. Orlov, V.I. Putlayev, P.V. Evdokimov, T.V. Safronova, A.V. Garshev, P.A. Milkin, Composite bioceramics engineering based on analysis of phase equilibria in the $Ca_3(PO_4)_2$–$CaNaPO_4$–$CaKPO_4$ system, Inorg. Mater. 55 (2019), https://doi.org/10.1134/S0020168519050157.
[10] N.K. Orlov, A.K. Kiseleva, P.A. Milkin, P.V. Evdokimov, V.I. Putlyaev, Reaction sintering of bioceramic based on substituted calcium phosphates $CaMPO_4$ (M = K, Na), Inorg. Mater. Appl. Res. 11 (2020) 394–402.
[11] A. Nadernezhad, F. Moztarzadeh, M. Hafezi, H. Barzegar-Bafrooei, Two step sintering of a novel calcium magnesium silicate bioceramic: sintering parameters and mechanical characterization, J. Eur. Ceram. Soc. 34 (2014) 4001–4009.
[12] K. Lin, J. Chang, Fabrication of dense hydroxyapatite nanobioceramics with enhanced mechanical properties via two-step sintering process, Appl. Ceram. Technol. 9 (2012) 479–485.
[13] K. Yoshida, M. Kobayashi, H. Hyuga, N. Kondo, H. Kita, K. Hashimoto, Y. Toda, Reaction sintering of b-tricalcium phosphates and their mechanical properties, J. Eur. Ceram. Soc. 27 (2007) 3215–3220.
[14] A. Cuccu, S. Montinaro, R. Orru, G. Cao, D. Bellucci, A. Sola, V. Cannillo, Consolidation of different hydroxyapatite powders by SPS: optimization of the sintering conditions and characterization of the obtained bulk products, Ceram. Int. 41 (2015) 725–736.
[15] L. Zhong, K. Aik, Transparent hydroxyapatite obtained through spark plasma sintering: optical and mechanical properties, Key Eng. Mater. 631 (2015) 51–56.
[16] B.-N. Kim, E. Prajatelistia, Y.-H. Han, H.-W. Son, Y. Sakka, S. Kim, Transparent hydroxyapatite ceramics consolidated by spark plasma sintering, Scripta Mater. 69 (2013) 366–369.
[17] K. Ioku, D. Kawagoe, H. Toya, H. Fujimori, S. Goto, K. Ishida, A. Mikuni, H. Mae, OH-designed transparent apatite ceramics prepared by spark plasma sintering, Trans. Mater. Res. Soc. Japan. 27 (2002) 447–449.
[18] Y.W. Gu, N.H. Loh, K.A. Khor, S.B. Tor, P. Cheang, Spark plasma sintering of hydroxyapatite powders, Biomaterials 23 (2002) 37–43.
[19] M. Cologna, J.S.C. Francis, R. Raj, Field assisted and flash sintering of alumina and its relationship to conductivity and MgO-doping, J. Eur. Ceram. Soc. 31 (2011) 2827–2837.
[20] M. Yu, S. Grasso, R. Mckinnon, T. Saunders, M.J. Reece, Review of flash sintering: materials, mechanisms and modelling, Adv. Appl. Ceram. 116 (2017) 24–60.
[21] M. Biesuz, V.M. Sglavo, Flash sintering of ceramics, J. Eur. Ceram. Soc. 39 (2019) 115–143.
[22] C.E.J. Dancer, Flash sintering of ceramic materials, Mater. Res. Express 3 (2016), 102001.
[23] I. Bajpai, Y.-H. Han, J. Yun, J. Francis, S. Kim, R. Raj, Preliminary investigation of hydroxyapatite microstructures prepared by flash sintering, Adv. Appl. Ceram. 115 (2016) 276–281.
[24] M.N. Rahaman, in: Ceramic Processing and Sintering, second ed., Marcek Dekker, Inc., New York, 2003.
[25] K. Maca, V. Pouchly, Z. Shen, Two-step sintering and spark plasma sintering of Al_2O_3, ZrO_2 and $SrTiO_3$ ceramics, Integrated Ferroelectrics Int. J. 99 (2008) 114–124.
[26] S.W. Wang, L.D. Chen, T. Hirai, Densification of Al2O3 powder using spark plasma sintering, J. Mater. Res. 15 (2000) 982–987.
[27] K. Ren, Q. Wang, Y. Lian, Y. Wang, Densification kinetics of flash sintered 3mol% Y_2O_3 stabilized zirconia, J. Alloys Compd. 747 (2018) 1073–1077.
[28] D. Liu, Y. Gao, J. Liu, K. Li, F. Liu, Y. Wang, L. An, SiC whisker reinforced ZrO_2 composites prepared by flash-sintering, J. Eur. Ceram. Soc. 36 (2016) 2051–2055.
[29] J.-C. M'Peko, C.J.S. Francis, R. Raj, Impedance spectroscopy and dielectric properties of flash versus conventionally sintered yttria-doped zirconia electroceramics viewed at the microstructural level, J. Am. Ceram. Soc. 96 (2013) 3760–3767.
[30] L. Mancuso, L. Desogus, R. Orrù, F. Loy, G. Cao, In-vitro behavior of different fully dense calcium phosphate materials fabricated by Spark Plasma Sintering, Ceram. Int. 43 (2017) 16238–16247, https://doi.org/10.1016/j.ceramint.2017.08.208.
[31] Z. Li, B.C. Thompson, Z. Dong, K.A. Khor, Optical and biological properties of transparent nanocrystalline hydroxyapatite obtained through spark plasma sintering, Mater. Sci. Eng. C 69 (2016) 956–966, https://doi.org/10.1016/j.msec.2016.08.002.
[32] D. Kawagoe, Y. Koga, N. Kotobuki, H. Ohgushi, E.H. Ishida, K. Ioku, Densification behavior of calcium phosphates on spark plasma sintering, Key Eng. Mater. 309–311 (2006) 171–174.
[33] M. Frasnelli, V.M. Sglavo, Flash sintering of tricalcium phosphate (TCP) bioceramics, J. Eur. Ceram. Soc. 38 (2018) 279–285, https://doi.org/10.1016/j.jeurceramsoc.2017.08.004.
[34] M. Frasnelli, A. Pedranz, M. Biesuz, S. Dire, V.M. Sglavo, Flash sintering of Mg-doped tricalcium phosphate (TCP) nanopowders, J. Eur. Ceram. Soc. 39 (2019) 3883–3892, https://doi.org/10.1016/j.jeurceramsoc.2019.05.007.
[35] F. Zhang, K. Lin, J. Chang, J. Lu, C. Ning, Spark plasma sintering of macroporous calcium phosphate scaffolds from nanocrystalline powders, J. Eur. Ceram. Soc. 28 (2008) 539–545, https://doi.org/10.1016/j.jeurceramsoc.2007.07.012.
[36] T. Znamierowska, Uklad $Ca_3(PO_4)_2$-$CaKPO_4$-$CaNaPO_4$. Czesc I, Zesz. Nauk. Politech. Sl. 709 (1982) 33–43.
[37] T. Znamierowska, Uklad $Ca_3(PO_4)_2$-$CaKPO_4$-$CaNaPO_4$. Czesc II, Zesz. Nauk. Politech. Sl. 709 (1982) 45–56.
[38] M.W. Barsoum, Fundamentals of Ceramics, IOP Publis, Cambridge University Press, 2003, https://doi.org/10.1088/1751-8113/44/8/085201.
[39] M.A. Clark, T.H. Alden, Deformation enchanced grain growth Sn-1% Bi alloy, Acta Metall. 21 (1973) 1195–1206.
[40] J. Besson, M. Abouaf, Grain growth enhancement in alumina during hot isostatic pressing, Acta Met. Mater. 39 (1991) 2225–2234.
[41] K.R. Venkatachari, R. Raj, Superplactic flow in fine-grained alumina, J. Am. Ceram. Soc. 38 (1986) 135–138.
[42] D.S. Wilkinson, C.H. Cacers, On the mechanism of strain-enchanced grain growth during superplastic deformation, Acta Metall. 32 (1984) 1335–1345.
[43] N.K. Orlov, V.I. Putlayev, P.V. Evdokimov, T.V. Safronova, E.S. Klimashina, P.A. Milkin, Resorption of $Ca_{3-x}M_{2x}(PO_4)_2$ (M = Na, K) calcium phosphate bioceramics in model solutions, Inorg. Mater. 54 (2018), https://doi.org/10.1134/S0020168518050096.
[44] R.I. Todd, E. Zapata-Solvas, R.S. Bonila, T. Sneddon, P.R. Wilshaw, Electrical characteristics of flash sintering: thermal runaway of Joule heating, J. Eur. Ceram. Soc. 35 (2015) 1865–1877.
[45] R. Chaim, Liquid film capillary mechanism for densification of ceramic powders during flash sintering, Materials 9 (2016) 280, https://doi.org/10.3390/ma9040280.
[46] M. Biesuz, L. Pinter, T. Saunders, M. Reece, J. Binner, V. Sglavo, S. Grasso, Investigation of electrochemical, optical and thermal effects during flash sintering of 8YSZ, Materials 11 (2018) 1214, https://doi.org/10.3390/ma11071214.
[47] T.P. Mishra, R.R.I. Neto, G. Speranza, A. Quaranta, V.M. Sglavo, R. Raj, O. Guillon, M. Bram, M. Biesuz, Electronic conductivity in gadolinium doped ceria under direct current as a trigger for flash sintering, Scripta Mater. 179 (2020) 55–60, https://doi.org/10.1016/j.scriptamat.2020.01.007.
[48] M. Biesuz, V.M. Sglavo, Microstructural temperature gradient-driven diffusion: possible densification mechanism for flash sintering of zirconia? Ceram. Int. 45 (2019) 1227–1236.
[49] J. Janek, J. Sann, B. Mogwitz, M. Rohnke, M. Kleine-Boymann, Degradation of functional materials in temperature gradients, J. Korean Ceram. Soc. 49 (2012) 56–65.
[50] B.S. Bokshtein, S.Z. Bokshtein, A.A. Zhukhovicki, Thermodynamics and Kinetic of Diffusion in Solid Body, Metallurgy, Moscow, 1974.
[51] H. Schmalzried, in: Chemical Kinetics of Solids, first ed., Wiley-VCH, 1995.